

Subaru HDS Transmission Spectroscopy of the Transiting Extrasolar Planet HD 209458b

Norio NARITA,¹ Yasushi SUTO,¹ Joshua N. WINN,^{2*} Edwin L. TURNER,^{1,3}
Wako AOKI,⁴ Christopher J. LEIGH,⁵ Bun'ei SATO,⁶ Motohide TAMURA,⁴ and Toru YAMADA,⁴

¹*Department of Physics, School of Science, The University of Tokyo, Tokyo 113-0033*
narita@utap.phys.s.u-tokyo.ac.jp, suto@phys.s.u-tokyo.ac.jp

²*Harvard-Smithsonian Center for Astrophysics,*
60 Garden St. MS-51, Cambridge, MA 02138, USA
jwinn@cfa.harvard.edu

³*Princeton University Observatory, Peyton Hall, Princeton, NJ 08544, USA*
elt@astro.princeton.edu

⁴*National Astronomical Observatory of Japan, 2-21-1, Mitaka, Tokyo 181-8588*
aoki.wako@nao.ac.jp, tamuramt@cc.nao.ac.jp
yamada@optik.mtk.nao.ac.jp

⁵*Liverpool John Moore's University, Astrophysics Research Institute,*
Twelve Quays House, Egerton Wharf, Birkenhead, CH41, 1LD, U.K.
cjl@astro.livjm.ac.uk

⁶*Graduate School of Science and Technology, Kobe University, 1-1 Rokkodai, Nada, Kobe 657-8501*
satobn@kobe-u.ac.jp

(Received 2005 March 7; accepted 2005 April 25)

Abstract

We have searched for absorption in several common atomic species due to the atmosphere or exosphere of the transiting extrasolar planet HD 209458b, using high precision optical spectra obtained with the Subaru High Dispersion Spectrograph (HDS). Previously we reported an upper limit on H α absorption of 0.1% (3σ) within a 5.1 Å band. Using the same procedure, we now report upper limits on absorption due to the optical transitions of Na D, Li, H α , H β , H γ , Fe, and Ca. The 3σ upper limit for each transition is approximately 1% within a 0.3 Å band (the core of the line), and a few tenths of a per cent within a 2 Å band (the full line width). The wide-band results are close to the expected limit due to photon-counting (Poisson) statistics, although in the narrow-band case we have encountered unexplained systematic errors at a few times the Poisson level. These results are consistent with all previously reported detections and upper limits, but are significantly more sensitive.

Key words: stars: planetary systems: individual (HD 209458b) — techniques: spectroscopic

1. Introduction

The first star other than the Sun for which a planetary transit was detected was HD 209458. The initial discovery by Charbonneau et al. (2000) and Henry et al. (2000), along with subsequent observations of higher accuracy by Brown et al. (2001) and Jha et al. (2000), allowed measurements of the orbital inclination ($i = 86^\circ.1$) and the planetary radius ($R = 1.34 R_{\text{Jup}}$). By combining these results with the stellar radial velocity data, it was shown that the companion has a mass comparable to Jupiter ($M = 0.69 M_{\text{Jup}}$) and the density of a gas giant planet ($\rho \sim 0.4 \text{ g cm}^{-3}$).

Observations of planetary transits also provide an opportunity to study the atmospheric properties of close-in giant extrasolar planets (also known as “hot Jupiters”). During occultations, a small fraction of the stellar disk is blocked from view, and an even smaller fraction of

the starlight is transmitted through the thin, partially-transparent portion of the planetary atmosphere and exosphere. Thus, by obtaining spectra with high spectral resolution and high signal-to-noise ratio, and comparing the spectra taken in and out of transit, one can detect absorption or emission features due to the planetary atmosphere or exosphere. This methodology is referred to as “transmission spectroscopy.”

Several studies of HD 209458 using transmission spectroscopy have previously been reported. Most have provided upper limits on particular absorption features. The first positive detection of an extrasolar planetary atmospheric absorption feature was made by Charbonneau et al. (2002). Their motivation was to confirm the prediction by Seager and Sasselov (2000) (and later, Brown 2001; Hubbard et al. 2001) of a relatively strong absorption feature in the sodium doublet lines. They observed HD 209458 with the Space Telescope Imaging Spectrograph (STIS) onboard the Hubble Space Telescope (HST), and found an additional $0.023 \pm 0.006\%$ absorp-

* Hubble Fellow.

tion during transits within a band pass centered on the sodium doublet lines ($5893 \pm 6 \text{ \AA}$). However, this additional absorption was significantly weaker than that predicted. Later, detection of excess absorption in the Ly α (1216 \AA) transition of neutral hydrogen was reported by Vidal-Madjar et al. (2003), also based on HST/STIS spectra. These authors found an amazingly strong additional Ly α absorption of $15 \pm 4\%$ during transits, implying that the absorbing H I gas extends over several planetary radii, and thus should be interpreted as an exosphere rather than an atmosphere. Vidal-Madjar et al. (2004) subsequently reported 2–3 σ detections of oxygen (O I) and carbon (C II) using HST/STIS. Interestingly, among the seven known cases of transiting hot Jupiters (Udalski et al. 2002a; Udalski et al. 2002b; Udalski et al. 2003; Alonso et al. 2004), HD 209458b has both the smallest mass and the largest radius, and thus an anomalously low density. This fact makes it yet more interesting to study the very extended exosphere of HD 209458b.

These reports of an extended exosphere around HD 209458b have inspired searches for additional absorption features. However, in spite of the successful detections via space-based observations, no data obtained from the ground has yet confirmed the detections or discovered any new components. Upper limits on planetary exospheric absorption features of various components in the optical region were reported by Bundy and Marcy (2000) based on Keck I/HIRES data. They obtained transmission spectra of HD 209458 (H β , H γ , Fe) and 51 Pegasi (Li, H α , Na D1, and D2), and placed upper limits of 3–20% on additional absorption during transits in a 0.3 \AA bandwidth centered on the cores of the relevant stellar lines. Moutou et al. (2001) also searched for transit effects (especially for ionized species) in the optical band with the VLT/UVES. They did not set upper limits on any specific atomic lines, but estimated a detection limit of order 1% within any 0.2 \AA band covered by the observations. Near-infrared features have also been examined to set more stringent upper limits on He, CO, H $_2$ O, and CH $_4$ (e.g. Brown et al. 2002; Harrington et al. 2002; Moutou et al. 2003; Deming et al. 2005).

In this paper we report on the results of searches for excess Na (D1, D2), Li, H β , H γ , Fe and Ca absorption in optical spectra of HD 209458 during transits, based on Subaru High Dispersion Spectrograph (HDS) data acquired in 2002 October. Compared with the previous investigations, the HDS data cover a larger range of wavelengths (covering the entire optical band) and have a higher signal-to-noise ratio. Moreover, this data set has a substantial advantage of covering a wide range of orbital phases, namely before, during and after the transit in a single night. The major obstacles to ground-based transmission spectroscopy are time-dependent effects due either to instrumental changes caused by variations in position, temperature et cetera, or to telluric effects such as seeing, airmass, and atmospheric absorption. All such effects are most effectively monitored, interpolated and removed if the data are obtained on a single night and if an entire transit is observed. We employed the same reduction and

analysis techniques used and described in detail in Winn et al. (2004) (hereafter Paper I) in which we set an upper limit of 0.1% (3σ) additional absorption in a 5.1 \AA band centered on H α .

This paper is organized as follows. Section 2 describes the observations, summarizes the reduction method and points out some small differences between the techniques employed in the present paper and Paper I. We present results for the selected absorption lines in section 3 and discuss systematic effects in section 4. Section 5 provides a brief summary and interpretation of the results.

2. Observations and Reduction Method

We observed HD 209458 on the nights of HST 2002 October 24 and 26 (25 and 27 in UT) with the Subaru HDS (Noguchi et al. 2002). The planet was predicted to transit its parent star near the middle of the night of HST October 24 (see figure 1), according to the ephemeris of Brown et al. (2001). In order to determine accurate radial velocities of the star and to verify the ephemeris, we obtained a spectrum with an Iodine Cell at both the start and the end of this series of exposures, and confirmed our expectation that the transit took place when predicted. We obtained 30 spectra of HD 209458, and 7 spectra of the rapidly rotating B5 Vn star HD 42545 (Abt et al. 2002) in order to evaluate the telluric spectrum. The wavelength coverage was $4100 \text{ \AA} < \lambda < 6800 \text{ \AA}$ with a spectral resolution of $R \approx 45000$ (0.9 km s^{-1} per pixel). The typical exposure time was 500 seconds with seeing of $\sim 0''.6$, through air masses ranging from 1.0 to 1.9. The resulting spectra had a typical signal-to-noise ratio of ≈ 350 per pixel.

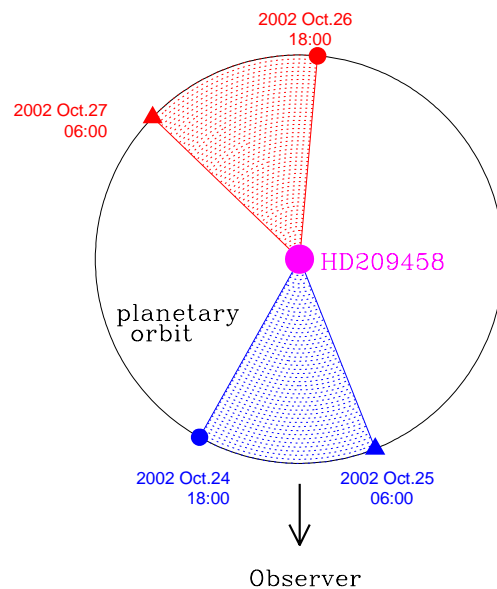


Fig. 1. Phase of the observations (times given in HST).

First, we processed the frames with standard IRAF¹ procedures and extracted one-dimensional spectra. Next, we applied an analysis method described at length in Paper I to correct for substantial time-dependent variations of the instrumental blaze function. However, a slight modification of the Paper I procedure was employed. In Paper I, we used all 4100 pixels of each spectral order to calculate the best-fitting parameters of a smooth function that describes the instrumental variations; however, we noted that this procedure acts to dilute any real signal. An artificially injected signal of 0.1% absorption was recovered with a strength of only 0.057%. We have since found that this problem is significantly reduced if the domain of pixels used in the fitting procedure is restricted to approximately 1000 pixels in the vicinity of the target line. This modification increases the sensitivity of the analysis and also provides a modestly improved correction for instrumental variations (see section 4).

Next, a template spectrum $T(\lambda)$ is created from all 30 individual exposures using the above correction method (see Paper I for further details). A time series of residual spectra are generated by subtracting the suitably matched template $T_m(\lambda)$ from each spectrum $S(\lambda, t)$; thus the template spectrum determines the zero-level for the residuals, and therefore we use all of the 30 spectra (including in-transit spectra) so as to create an optimum template spectrum. Then, we examine the time variation of each selected absorption line in order to search for possible additional absorption in the transit phase. Specifically, we compute a time series of fractional difference in flux between the spectrum and the matched template within a smoothing width $\Delta\lambda$ according to

$$\delta_A(t) = \frac{\int_{\lambda_0 - \Delta\lambda/2}^{\lambda_0 + \Delta\lambda/2} d\lambda [S(\lambda, t) - T_m(\lambda)]}{\int_{\lambda_0 - \Delta\lambda/2}^{\lambda_0 + \Delta\lambda/2} d\lambda T_m(\lambda)}, \quad (1)$$

where A indicates each target absorption line. We refer to such a time variation of the fractional difference as a “difference light curve”.

To place a quantitative limit on additional absorption, we calculate $\bar{\delta}_{\text{in},A}$ and $\sigma_{\text{in},A}$:

$$\bar{\delta}_{\text{in},A} \equiv \frac{1}{N_{\text{in}}} \sum_{t=\text{in}} \delta_A(t), \quad (2)$$

$$\sigma_{\text{in},A} \equiv \sqrt{\frac{1}{N_{\text{in}}} \sum_{t=\text{in}} [\bar{\delta}_{\text{in},A} - \delta_A(t)]^2}, \quad (3)$$

which are the mean value and the standard deviation of $\delta_A(t)$ for the spectra taken in the transit (between second and third contacts, namely within ± 60 minutes from center of the transit). Similarly, we compute $\bar{\delta}_{\text{out},A}$ and $\sigma_{\text{out},A}$ from the spectra taken out of the transit (before

first contact or after fourth contact: beyond ± 92 minutes from center of the transit).² The numbers of spectra in each phase are $N_{\text{in}} = N_{\text{out}} = 12$.

Finally, we compute

$$\bar{\delta}_A \equiv \bar{\delta}_{\text{in},A} - \bar{\delta}_{\text{out},A}, \quad (4)$$

$$\sigma_A \equiv \sqrt{\frac{N_{\text{in}}\sigma_{\text{in},A}^2 + N_{\text{out}}\sigma_{\text{out},A}^2}{N_{\text{in}} + N_{\text{out}}}} = \sqrt{\frac{\sigma_{\text{in},A}^2 + \sigma_{\text{out},A}^2}{2}}. \quad (5)$$

Note that $\bar{\delta}_A$ would be negative if there were additional absorption during transit.

In the following sections, we express the results as $\bar{\delta}_A \pm \sigma_A$. Where no additional absorption feature related to transit are detected (i.e., $|\bar{\delta}_A| < \sigma_A$), we quote upper limits as $3\sigma_A$.

3. Results

Since the HDS spectra cover a wide wavelength region in optical band (4100 – – 6800 Å), there are many absorption lines available for inspection. We concentrate on the following transitions for detailed study: 1) the sodium and lithium lines, because additional absorptions at these lines are theoretically predicted by Seager and Sasselov (2000); 2) neutral hydrogen lines including H α , H β , and H γ , since an extended hydrogen exosphere was reported by Vidal-Madjar et al. (2003); and 3) the strong stellar lines of Ca and Fe. Another reason to examine the sodium doublet lines in detail is to attempt to confirm the report by Charbonneau et al. (2002) of additional $0.023 \pm 0.006\%$ absorption in the 5893 ± 6 Å band.

In Paper I, we paid particular attention to the results for a bandwidth of 5.1 Å, in order to facilitate a comparison with the band used by Vidal-Madjar et al. (2003). In this work we generally consider two different bandwidths: a relatively narrow band of 0.3 Å [so as to facilitate comparison with the previous results of Bundy and Marcy (2000) and Moutou et al. (2001)], and a relatively wide band of 2 Å to cover the full width of target absorption lines and provide more sensitivity.

3.1. Calculation of Difference Spectra

We express the difference between each spectrum and the matched template in units of the expected standard deviation due to Poisson statistics,

$$\frac{S(\lambda) - T_m(\lambda)}{\sqrt{T_m(\lambda)}}, \quad (6)$$

and refer to this quantity as a “difference spectrum”. As an example, the difference spectra in the vicinity of the sodium resonance doublet are shown in figure 2. The template spectrum and the telluric spectrum are plotted at the bottom of the series. To estimate the telluric spectrum, we created a template spectrum for HD 42545 in

¹ The Image Reduction and Analysis Facility (IRAF) is distributed by the U.S. National Optical Astronomy Observatories, which are operated by the Association of Universities for Research in Astronomy, Inc., under cooperative agreement with the National Science Foundation.

² To compute the transit times, we use an ephemeris defined by J.D. (mid-transit) = 2451659.93675 (Brown et al. 2001) and the most precise published period, $P = 3.524739$ d (Robichon and Arenou 2000).

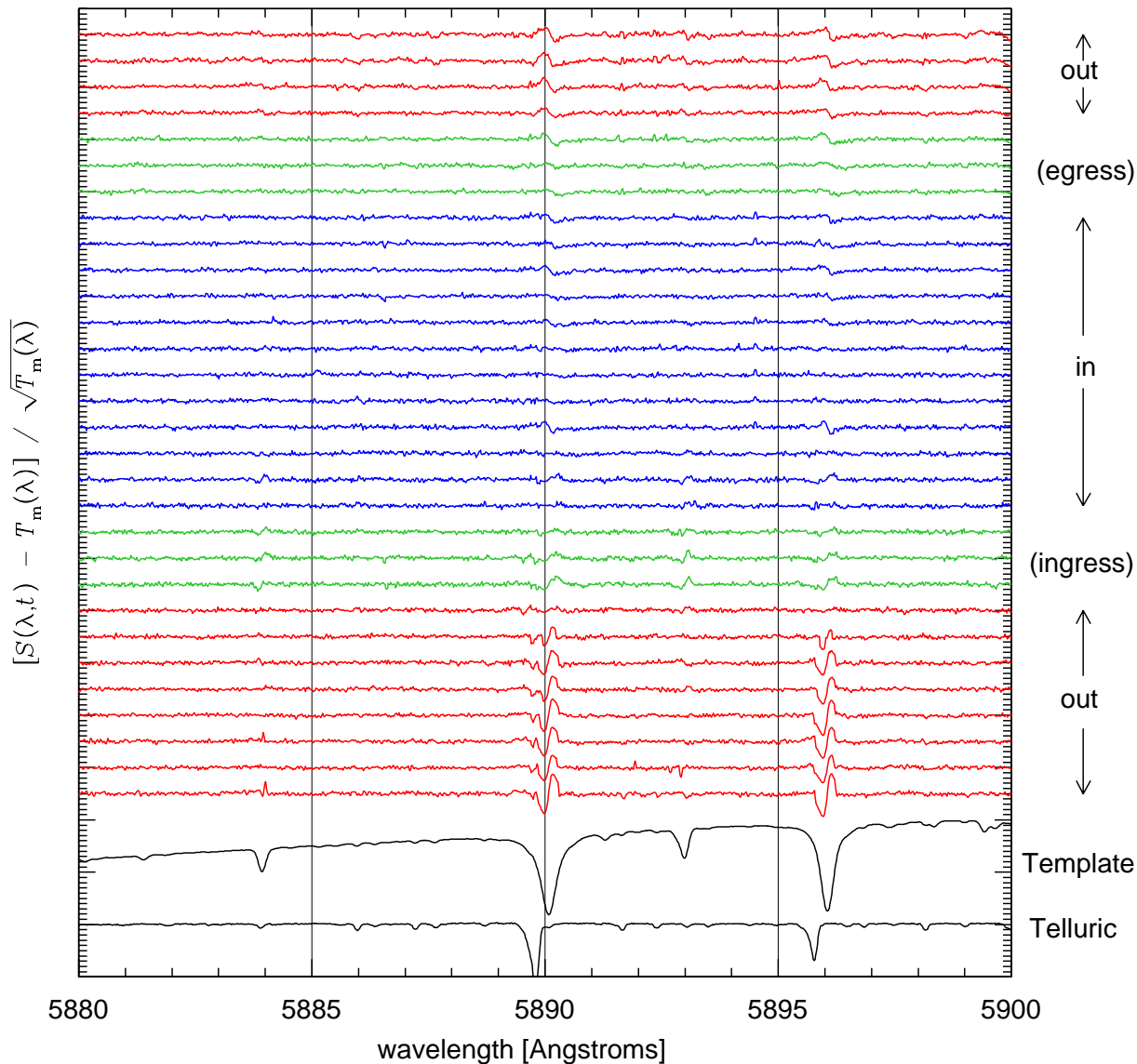


Fig. 2. Difference between each spectrum and its matched template for a wavelength range in the vicinity of the sodium doublet lines. The spectra are ordered in time from bottom to top. The corresponding phases of the planetary transit are noted on the right side of the figure. The spacing between minor ticks represents two Poisson deviations. The bottom spectrum shows the normalized template spectrum of the rapidly rotating star HD 42545, containing telluric features and interstellar sodium absorption. The second spectrum shows the overall template spectrum of HD 209458. Note that we do not correct to the laboratory frame.

the same way as for HD 209458 and normalized it appropriately for visual reference.

The template spectrum shows some features that are similar to those seen in the estimated telluric spectrum. However, the latter spectrum is in reality not just the telluric spectrum; it is also affected by interstellar sodium absorption. Moreover, the sodium D2 line at 5890 Å is blended with strong telluric vapor absorption (e.g., Lundstrom et al. 1991), and the variation of mesospheric sodium column density is not negligible (e.g., Ge et al. 1997). These factors substantially complicate any interpretation of the observed Na lines.

There are time-dependent, coherent features with amplitudes that are in excess of the Poisson noise level in the vicinity of the Na lines (such features are also seen for

other lines, but at a much reduced level). These anomalies strongly resemble those which would be produced by a small, time-dependent wavelength shift. However, measurements of the line center wavelengths (obtained by fitting a Gaussian function to the line profile) of both stellar and telluric features show them to be stable to within ± 0.01 Å (less than 1 pixel), and show no systematic drift with time. Thus, they do not appear to be directly associated with errors or drift in our wavelength calibration (determined from Thorium–Argon lamp spectra obtained at the beginning and end of the HD 209458 exposures). Furthermore, these features are strongest *outside* of the transit phase, especially at the beginning of the observation when the target was near zenith, and thus when the instrument was rotating most rapidly. Hence, we believe

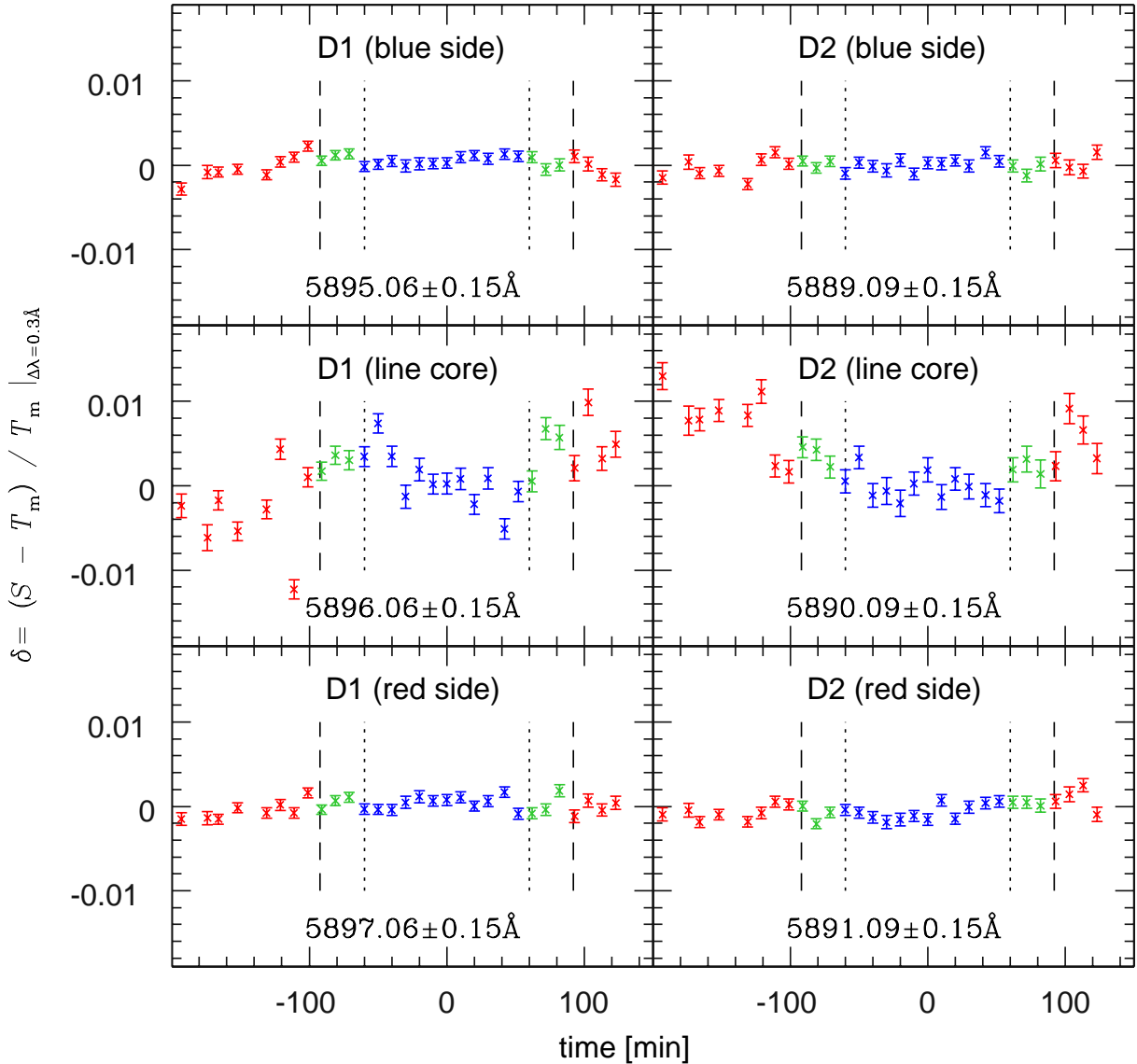


Fig. 3. Difference light curves around the sodium doublet lines for a smoothing width of $\Delta\lambda = 0.3 \text{ \AA}$. The error bars represent the Poisson noise $\sqrt{T_m}$, and the horizontal axis indicates the time of each exposure with the origin at mid-transit. The time between the two dotted lines indicates the in-transit phase, and those between the dashed line and dotted line show ingress (left side) and egress (right side) phases. The left side panels exhibit difference light curves for the Na D1 line at $5895.06 \pm 0.15 \text{ \AA}$ (top panel; continuum of blue side), $5896.06 \pm 0.15 \text{ \AA}$ (middle panel; line core), $5897.06 \pm 0.15 \text{ \AA}$ (bottom panel; continuum of red side). The right side panels are similar, but for the Na D2 line; $5889.09 \pm 0.15 \text{ \AA}$ (top panel; continuum of blue side), $5890.09 \pm 0.15 \text{ \AA}$ (middle panel; line core), $5891.09 \pm 0.15 \text{ \AA}$ (bottom panel; continuum of red side).

the anomalies are unlikely to be due to real absorption in the HD 209458 system. Whatever their source, these features appear to have almost exactly zero net photon count; they cancel out almost completely when integrated over a smoothing width comparable to the overall line width (e.g., 2 \AA). This suggests that they do not compromise the achieved detection sensitivity for such a bandwidth.

3.2. Comparison with Previous Results

The same analysis was applied to the other selected lines. For the other lines, there was no significant interstellar absorption contamination such as that observed for Na. In order to compare our results with previous

ones, we selected a bandwidth matched to past studies. In particular we followed the conventions of Bundy and Marcy (2000), who performed transmission spectroscopy for HD 209458 and 51 Pegasi in various atomic lines. They used $\Delta\lambda \simeq 0.3 \text{ \AA}$ in order to emphasize the line cores.

The time variations of the fractional difference for $\Delta\lambda = 0.3 \text{ \AA}$ at the sodium doublet lines are plotted in figure 3. It is evident that the difference light curves for continuum regions are nearly consistent with the Poisson noise of $\sim 0.07\%$, while those for line cores have a significantly larger scatter than the expected Poisson noise of $\sim 0.15\%$. The results for line cores are $\delta_{D1} = 0.12 \pm 0.48\%$ and $\delta_{D2} = -0.70 \pm 0.28\%$, respectively. Although δ_{D2} indicates

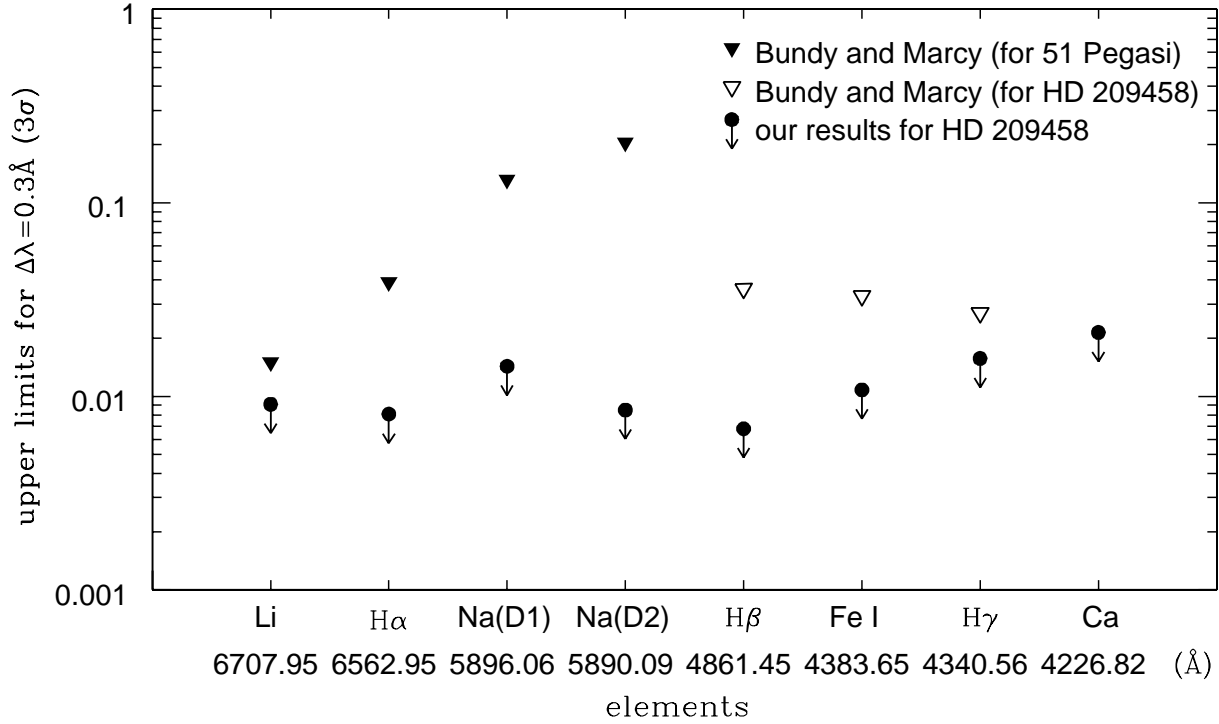


Fig. 4. Comparison of the Subaru HDS upper limits for $\Delta\lambda = 0.3 \text{ \AA}$ with those of Bundy and Marcy (2000). The vertical axis is fractional upper limits on additional absorption during transit on a log scale. The horizontal axis indicates atomic species and corresponding line wavelength λ_0 in equation (1). Note that Bundy and Marcy (2000) did not report a Ca (4226.82 \AA) result, and their upper limits on Li, H α , and Na (D1, D2) are for 51 Pegasi.

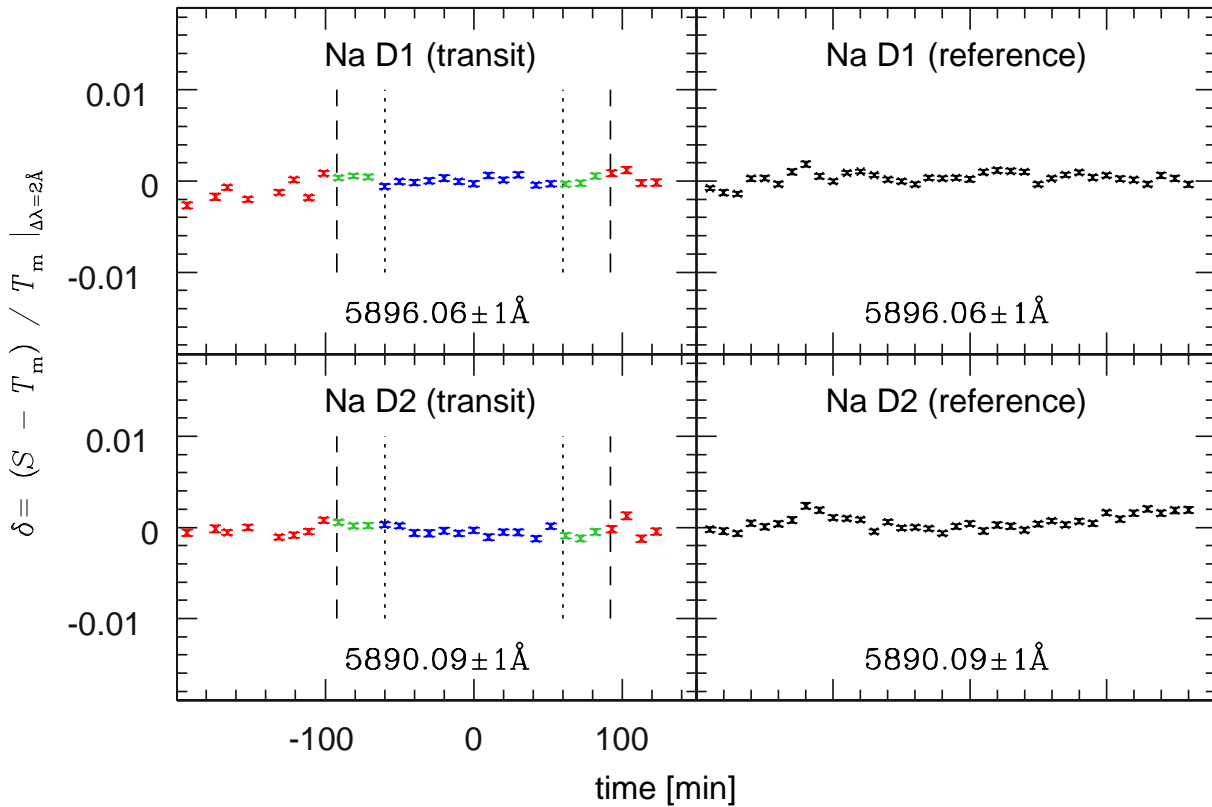


Fig. 5. Difference light curves for $\Delta\lambda = 2 \text{ \AA}$ around the sodium doublet. The left panels exhibit the light curves on the transiting night (the night of HST 2002 October 24), and the right panels are those for the out-of-transit night (October 26). The vertical scale is matched to that of figure 3.

a 2.5σ detection of additional absorption, δ_{D1} does not exhibit a corresponding signal, and as noted at the end of the previous subsection, the difference spectra have unexplained systematic anomalies on a wavelength scale larger than the 0.3 \AA smoothing region. Thus, we do not regard this 2.5σ signal as real absorption, but rather as an indicator of systematic error. The resulting upper limits are $3\sigma_{D1} = 1.43\%$ and $3\sigma_{D2} = 0.85\%$.

Figure 4 shows a comparison of our upper limits for HD 209458 with those of Bundy and Marcy (2000) for HD 209458 (H β , H γ , Fe) and 51 Pegasi (Li, H α , Na D1, and D2). Note that although 51 Pegasi does not show transits, they consider that the lack of transits does not rule out the possibility of excess absorption features. The Subaru HDS upper bounds are the most stringent limits so far that have been obtained with ground-based observations in the optical region.

3.3. Results for Integration over the Full Line Width

We repeated the same procedure described in the previous subsection using a smoothing width $\Delta\lambda = 2 \text{ \AA}$ in order to cover the typical width of the strong stellar absorption lines. In this case, the contribution from the small systematic features discussed in subsection 3.1 was nearly zero, because of the inversion symmetry of those anomalies. We display the difference light curves of the Na D lines in figure 5, as examples. The large scatter seen in figure 3 is almost entirely removed for this larger smoothing width. The results are $\delta_{D1} = 0.06 \pm 0.09\%$ and $\delta_{D1} = -0.02 \pm 0.06\%$. We also plot $\delta(t)$ for the out-of-transit data obtained on the night of HST 2002 October 26 for reference (right side). These panels exhibit very similar variations to those in the October 24 data, and thus support the conclusion of no detected additional absorption during the transit event.

Our fractional upper limits on additional absorption during transit for all of the selected lines and both values of $\Delta\lambda$ lines are given in table 1. We did not set upper limits on Fe I and Ca I in blue CCD, since the bands of $\Delta\lambda = 2 \text{ \AA}$ contain several irrelevant absorption lines.

We also derived an upper limit on the Na D lines with $\Delta\lambda = 12 \text{ \AA}$, corresponding to the band in which Charbonneau et al. (2002) reported detection of additional absorption ($5893 \pm 6 \text{ \AA}$). The resulting difference light curve is plotted in figure 6, and the result is $\delta_{Na} = 0.03 \pm 0.04\%$. Thus, we are not able to either confirm or contradict the additional absorption of 0.02% reported by Charbonneau et al. (2002), since it is beyond our sensitivity level.

4. Evaluation of Systematic Errors

In order to evaluate the significance of high precision measurements, such as those presented in this paper and to facilitate the planning of similar, future observations, it is necessary to thoroughly understand the sources and magnitudes of systematic errors.

We therefore carried out further analyses of the remaining systematic effects, such as instrumental variations and

Table 1. Summary of the 3σ upper limits.

Element	λ_0 (\AA)	$\Delta\lambda = 0.3 \text{ \AA}$ (%)	$\Delta\lambda = 2 \text{ \AA}$ (%)
red CCD			
Li I	6707.95	0.91	0.43
H α	6562.95	0.81	0.66
Fe I	6024.20	0.84	0.18
Na I(D1)	5896.06	1.43	0.28
Na I(D2)	5890.09	0.85	0.18
blue CCD			
H β	4861.45	0.68	0.34
Fe I	4383.65	1.08	—
H γ	4340.56	1.57	0.88
Ca I	4226.82	2.14	—

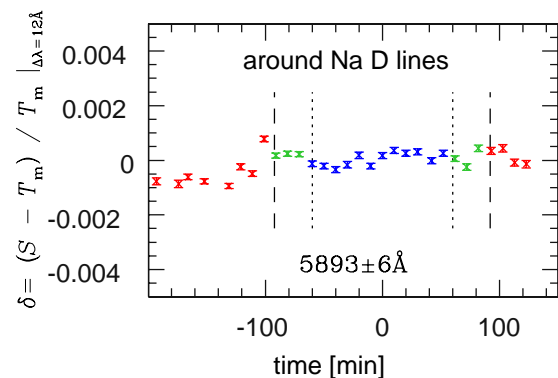


Fig. 6. Difference light curve for $5893 \pm 6 \text{ \AA}$, corresponding to the band in which Charbonneau et al. (2002) reported the detection of 0.02% additional absorption.

telluric effects, which may be serious obstacles to improving ground-based observations. First of all, we checked the reliability of our correction method for the instrumental variations and estimated the magnitude of any remaining instrumental effects on the results. Next, we confirmed that the correction method does not dilute any real signal which is above the Poisson noise limit. Finally, we analyzed the correlation between the spectra of HD 209458 and rapidly rotating star HD 42545 in order to estimate the influence of terrestrial atmospheric effects.

4.1. Estimation of Instrumental Effects

Although our spectrum-matching procedure (Paper I gives its details) is intended to correct for instrumental variations, the correction is not perfect. To estimate the size of the remaining instrumental effects, we selected an appropriate reference absorption line on the red CCD. We adopted the Fe I] (intercombination) line at 6024.20 \AA for the following reasons: (i) there are no telluric lines within $\pm 2 \text{ \AA}$ (Moore et al. 1966), and (ii) the position of the line is near the peak of the continuum, which minimizes the Poisson noise level. The same procedure described in the previous section was applied with $\Delta\lambda = 0.3 \text{ \AA}$ and 2 \AA to the band around 6024.20 \AA .

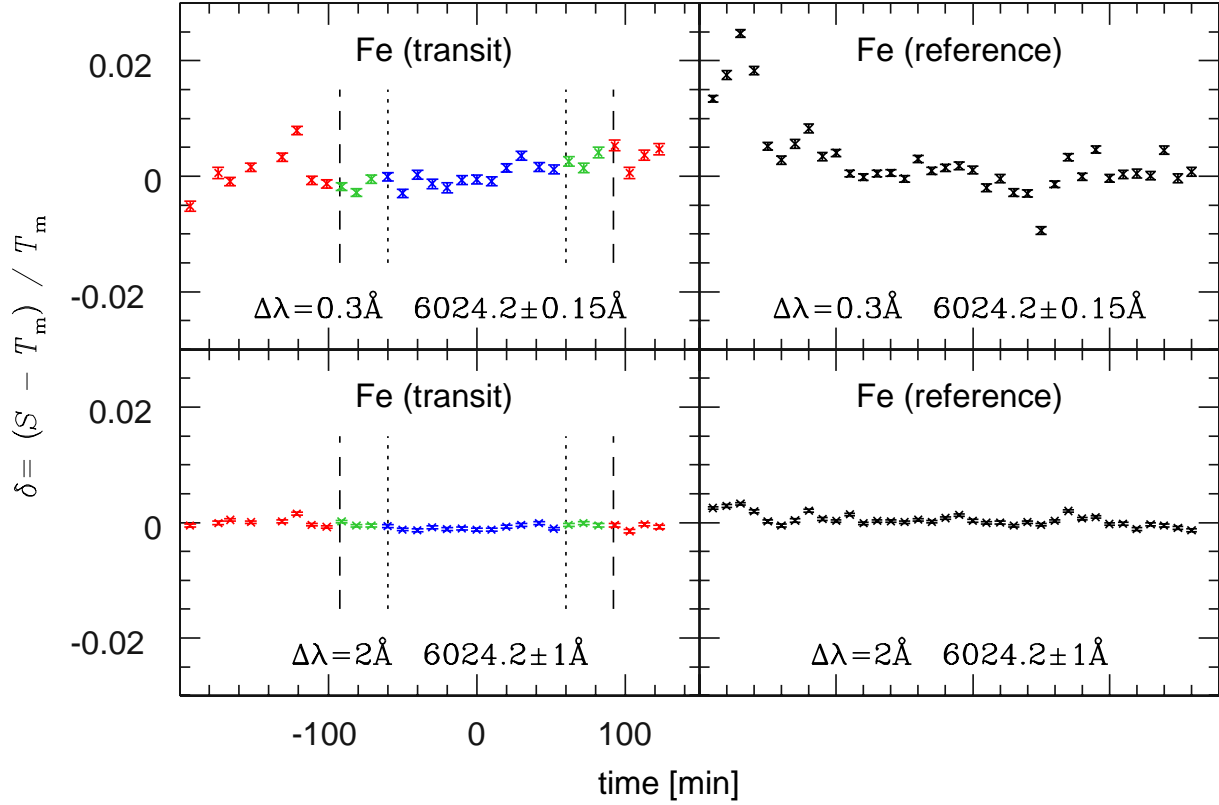


Fig. 7. Difference light curves for the reference Fe line at 6024 Å. The upper panels show fractional differences of $\Delta\lambda = 0.3$ Å, while the lower panels use $\Delta\lambda = 2$ Å. The standard deviations are 0.28% (upper left), 0.65% (upper right), 0.06% (lower left), and 0.10% (lower right) respectively.

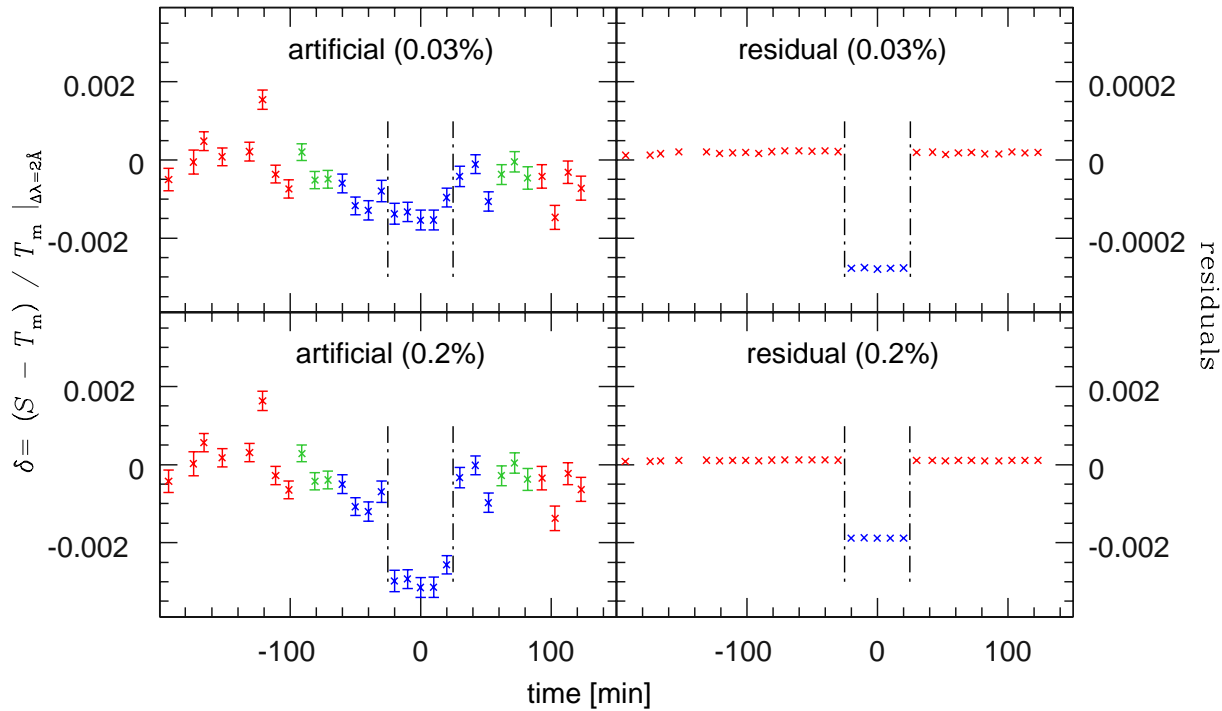


Fig. 8. Difference light curves with artificial absorption (left panels). The five data points between the dot-dashed lines indicate the results with artificial signals. The left panels show its recovery via our analysis procedure, and the right panels show residuals that subtracted the original difference light curve (lower left panel of figure 7.) from the left panels.

The difference light curves are shown in figure 7, and have standard deviations of 0.28% (upper left), 0.65% (upper right), 0.06% (lower left), and 0.10% (lower right). As suggested by the analysis presented in the previous sections, instrumental variations appear to be removed approximately within the Poisson noise limit for the larger value of $\Delta\lambda$ that integrates over the whole line width. However, for the narrower band, which includes only the line core, systematic effects of unknown origin increase the effective noise to a level that is several times larger than the expected Poisson noise.

4.2. Recovery of Artificial Input Signals

In order to verify that our reduction and analysis procedures do not remove or dilute real signals, we injected an artificial signal of 0.03% (corresponding to the Poisson noise) and 0.2% into 5 out of 30 spectra in the October 24 data around 6024 ± 1 Å, and analyzed it via the same methods. Figure 8 shows difference light curves for $\Delta\lambda = 2$ Å (left side) and residuals that subtracted the original difference light curve from left panels (right side). We compared the mean and standard deviation of 25 realizations without artificial injection ($\delta_{\text{no}}, \sigma_{\text{no}}$), and 5 with artificial signals injected ($\delta_{\text{art}}, \sigma_{\text{art}}$). We find that the residual $(\delta_{\text{no}} - \delta_{\text{art}}) \pm (\sqrt{25\sigma_{\text{no}}^2/30 + 5\sigma_{\text{art}}^2/30})$ values are $0.0296 \pm 0.0003\%$ (originally 0.03%) and $0.1987 \pm 0.0009\%$ (originally 0.2%). We thus conclude that the procedures used in this paper can recover small input signals over the Poisson noise limits with $\Delta\lambda = 2$ Å quite satisfactorily and without significant dilution.

4.3. Telluric Effects

Spectra obtained from the ground naturally contain many telluric absorption features. We obtained spectra of the rapidly rotating star HD 42545 at the end of the night (airmass ~ 1.9) and used this data to identify many such lines listed in Moore et al. (1966). Many telluric water vapor and oxygen absorption lines are visible in the spectra of the red CCD, particularly.

The difference light curves for one strong telluric oxygen line at 6287.75 Å with both $\Delta\lambda = 0.3$ Å (top panel) and $\Delta\lambda = 2$ Å (middle panel) are shown in figure 9. The bottom panel shows the difference light curve for 5885.98 ± 0.15 Å, which contains one of the strongest telluric water vapor lines near the Na D doublet, although it is 5 to 10 times weaker than the 6287.75 Å oxygen line. These plots show that the telluric features are measured to roughly within the Poisson noise (as expected), and do not exhibit any anomalous behavior during the transit phase, and vary most strongly at the end of the night when the air mass became considerable (~ 2.0).

Based on these results we estimate the telluric water vapor contamination levels by comparison with the equivalent widths listed in Moore et al. (1966), and conclude that they were no more than 0.5% for $\Delta\lambda = 0.3$ Å, and less than 0.1% (3σ) for $\Delta\lambda = 2$ Å for all of the lines listed in table 1.

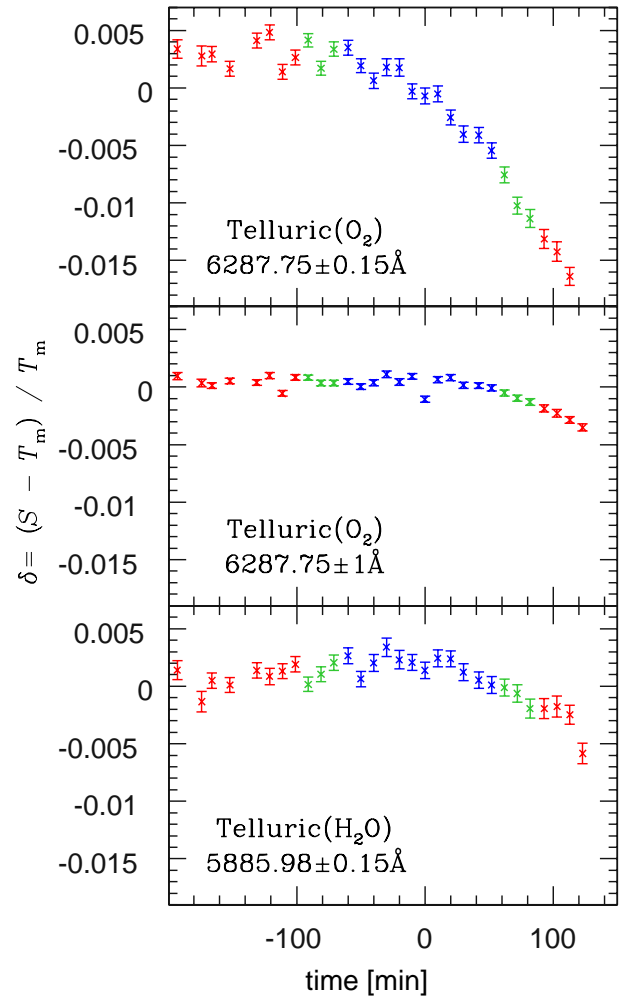


Fig. 9. Difference light curves of a telluric oxygen line (upper and middle) and a water vapor feature (lower; near the Na D doublet). The strengths of both features increased near the end of the night when the air mass became significantly larger with time.

5. Summary and Conclusions

An investigation of the optical spectra taken during a transit of the HD 209458 system with Subaru HDS revealed no additional absorption features associated with the transit. The typical achieved sensitivity level is $\sim 1\%$ (3σ) for $\Delta\lambda = 0.3$ Å (the line cores) in fractional difference spectra, and a few times smaller for $\Delta\lambda = 2$ Å (the full line width). Although we cannot confirm the smaller level of absorption in the Na D line that was observed from space (Charbonneau et al. 2002), our upper limits for the other optical transitions are consistent with, but more stringent than, those previously achieved from the ground.

Given the systematic effects that we encountered when working at very high precision, one may wonder whether ground-based observations can ever be competitive with space-based observations for this purpose. The answer is unclear, but there are at least a few lines of future research that may help to improve the prospects for ground-based

observations. As we have argued, the primary obstacle to higher-precision differential spectroscopy seems to be small temporal variations in instrumental response; telluric contamination is not negligible, but is removable to some extent. Instruments that are purpose-built for increased stability (despite telescope motion and instrument rotation) may be required. Alternatively, it may be possible to use the multi-object capability of some spectrographs to record simultaneous high-resolution, high-SNR spectra of additional objects besides the exoplanetary system, and perform differential spectrophotometry. Finally, an alternative method for probing exoplanetary atmospheres was recently proposed by Snellen (2004). The idea is to measure the line-dependence of the Rossiter-McLaughlin effect (e.g., Rossiter 1924; McLaughlin 1924; Queloz et al. 2000; Ohta et al. 2005), which is the spectral line distortion caused by the planet since it blocks a particular part of the rotation field of the face of the star. This method involves a comparison of the shapes of different spectral lines, rather than their depths relative to the continuum. Thus using this method in ground-based observations is quite reasonable, because ground-based instruments would not exceed space-based ones in photometric accuracy, but possibly could do so in spectral resolution. We intend to use the existing Subaru/HDS data to investigate this latter possibility.

We are very grateful to Kozo Sadakane for helpful advice concerning telluric contamination. We also acknowledge close support of our observations by Akito Tajitsu, who is a Support Astronomer of Subaru HDS. This work is based on data from Subaru Telescope which is operated by the National Astronomical Observatory of Japan, and supported in part by a Grant-in-Aid for Scientific Research from the Japan Society for Promotion of Science (No.14102004, 16340053), and by NASA grant NAG5-13148. The visit of E.L.T at the University of Tokyo is supported by an invitation fellowship program for research in Japan from JSPS. Work by J.N.W. is supported by NASA through Hubble Fellowship grant HST-HF-01180.02-A, awarded by the Space Telescope Science Institute, which is operated by the Association of Universities for Research in Astronomy, Inc., for NASA, under contract NAS 5-26555. M.T. acknowledges support by Grant-in-Aids on Priority Area No. 160777204 of the Ministry of Education, Culture, Sports, Science and Technology of Japan. We wish to recognize and acknowledge the very significant cultural role and reverence that the summit of Mauna Kea has always had within the indigenous Hawaiian community. We are most fortunate to have had the opportunity to conduct observations from this mountain.

References

- Abt, H. A., Levato, H., & Grosso, M. 2002, *ApJ*, 573, 359
 Alonso, R., et al. 2004, *ApJ*, 613, L153
 Brown, T. M. 2001, *ApJ*, 553, 1006
 Brown, T. M., Charbonneau, D., Gilliland, R. L., Noyes, R. W., & Burrows, A. 2001, *ApJ*, 552, 699
 Brown, T. M., Libbrecht, K. G., & Charbonneau, D. 2002, *PASP*, 114, 826
 Bundy, K. A., & Marcy, G. W. 2000, *PASP*, 112, 1421
 Charbonneau, D., Brown, T. M., Latham, D. W., & Mayor, M. 2000, *ApJ*, 529, L45
 Charbonneau, D., Brown, T. M., Noyes, R. W., & Gilliland, R. L. 2002, *ApJ*, 568, 377
 Deming, D., Brown, T. M., Charbonneau, D., Harrington, J., & Richardson, L. J. 2005, *ApJ*, 622, 1149
 Ge, J., et al. 1997, astro-ph/9708275
 Harrington, J., Deming, D., Matthews, K., Richardson, L. J., Rojo, P., Steyert, D., Wiedemann, G., & Zeehandelaar, D. 2002, *BAAS*, 34, 1175
 Henry, G. W., Marcy, G. W., Butler, R. P., & Vogt, S. S. 2000, *ApJ*, 529, L41
 Hubbard, W. B., Fortney, J. J., Lunine, J. I., Burrows, A., Sudarsky, D., & Pinto, P. 2001, *ApJ*, 560, 413
 Jha, S., Charbonneau, D., Garnavich, P. M., Sullivan, D. J., Sullivan, T., Brown, T. M., & Tonry, J. L. 2000, *ApJ*, 540, L45
 Lundstrom, I., Ardeberg, A., Maurice, E., & Lindgren, H. 1991, *A&AS*, 91, 199
 McLaughlin, D. B. 1924, *ApJ*, 60, 22
 Moore, C. E., Minnaert, M. G. J., & Houtgast, J. 1966, *The solar spectrum 2935 Å to 8770 Å (National Bureau of Standards Monograph (Washington: US Government Printing Office))*
 Moutou, C., Coustenis, A., Schneider, J., St Gilles, R., Mayor, M., Queloz, D., & Kaufer, A. 2001, *A&A*, 371, 260
 Moutou, C., Coustenis, A., Schneider, J., Queloz, D., & Mayor, M. 2003, *A&A*, 405, 341
 Noguchi, K., et al. 2002, *PASJ*, 54, 855
 Ohta, Y., Taruya, A., & Suto, Y. 2005, *ApJ*, 622, 1118
 Queloz, D., Eggenberger, A., Mayor, M., Perrier, C., Beuzit, J. L., Naef, D., Sivan, J. P., & Udry, S. 2000, *A&A*, 359, L13
 Robichon, N., & Arenou, F. 2000, *A&A*, 355, 295
 Rossiter, R. A. 1924, *ApJ*, 60, 15
 Seager, S., & Sasselov, D. D. 2000, *ApJ*, 537, 916
 Snellen, I. A. G. 2004, *MNRAS*, 353, L1
 Udalski, A., et al. 2002a, *Acta Astron.*, 52, 1
 Udalski, A., Zebun, K., Szymanski, M., Kubiak, M., Soszynski, I., Szewczyk, O., Wyrzykowski, L., & Pietrzynski, G. 2002b, *Acta Astron.*, 52, 115
 Udalski, A., Pietrzynski, G., Szymanski, M., Kubiak, M., Zebun, K., Soszynski, I., Szewczyk, O., & Wyrzykowski, L. 2003, *Acta Astron.*, 53, 133
 Vidal-Madjar, A., Lecavelier des Etangs, A., Désert, J.-M., Ballester, G. E., Ferlet, R., Hébrard, G., & Mayor, M. 2003, *Nature*, 422, 143
 Vidal-Madjar, A., et al. 2004, *ApJ*, 604, L69
 Winn, J. N., Suto, Y., Turner, E. L., Narita, N., Frye, B. L., Aoki, W., Sato, B., & Yamada, T. 2004, *PASJ*, 56, 655 (Paper I)